Improved measurement of *CP*-violation parameters $\sin 2\phi_1$ and $|\lambda|$, B meson lifetimes, and B^0-$\overline{B}^0$ mixing parameter Δm_d

K. Abe,[8] K. Abe,[41] I. Adachi,[8] H. Aihara,[43] M. Akatsu,[21] Y. Asano,[47] T. Aushev,[12] T. Aziz,[39] S. Bahinipati,[4] A. M. Bakich,[38] Y. Ban,[32] S. Banerjee,[39] A. Bay,[17] I. Bedny,[1] U. Bitenc,[13] I. Bizjak,[13] S. Blyth,[25] A. Bondar,[1] A. Bozek,[26] M. Bračko,[8,19,13] J. Brodzicka,[26] T. E. Browder,[7] P. Chang,[25] Y. Chao,[25] A. Chen,[23] K.-F. Chen,[25] W. T. Chen,[23] B. G. Cheon,[3] R. Chistov,[12] S.-K. Choi,[6] Y. Choi,[37] A. Chuvikov,[33] S. Cole,[38] J. Dalseno,[20] M. Danilov,[12] M. Dash,[48] A. Drutskoy,[4] S. Eidelman,[1] V. Eiges,[12] F. Fang,[7] S. Fratina,[13] N. Gabyshev,[1] A. Garmash,[33] T. Gershon,[8] A. Go,[23] G. Gokhroo,[39] B. Golob,[18,13] J. Haba,[8] K. Hara,[8] N. C. Hastings,[8] K. Hayasaka,[21] H. Hayashii,[22] M. Hazumi,[8] I. Higuchi,[42] T. Higuchi,[8] L. Hinz,[17] T. Hokuue,[21] Y. Hoshi,[41] S. Hou,[23] W.-S. Hou,[25] T. Iijima,[21] A. Imoto,[22] K. Inami,[21] A. Ishikawa,[8] H. Ishino,[44] R. Itoh,[8] Y. Iwasaki,[8] H. Kakuno,[43] J. H. Kang,[49] J. S. Kang,[15] P. Kapusta,[26] S. U. Kataoka,[22] N. Katayama,[8] H. Kawai,[2] T. Kawasaki,[28] H. Kichimi,[8] H. J. Kim,[16] J. H. Kim,[37] S. K. Kim,[36] S. M. Kim,[37] K. Kinoshita,[4] P. Koppenburg,[8] S. Korpar,[19,13] P. Križan,[18,13] P. Krokovny,[1] C. C. Kuo,[23] Y.-J. Kwon,[49] J. S. Lange,[5] G. Leder,[11] S. H. Lee,[36] T. Lesiak,[26] J. Li,[35] S.-W. Lin,[25] D. Liventsev,[12] J. MacNaughton,[11] G. Majumder,[39] F. Mandl,[11] D. Marlow,[33] T. Matsumoto,[45] A. Matyja,[26] W. Mitaroff,[11] K. Miyabayashi,[22] H. Miyake,[30] H. Miyata,[28] R. Mizuk,[12] T. Nagamine,[42] Y. Nagasaka,[9] I. Nakamura,[8] E. Nakano,[29] M. Nakao,[8] S. Nishida,[8] O. Nitoh,[46] S. Noguchi,[22] T. Nozaki,[8] S. Ogawa,[40] T. Ohshima,[21] T. Okabe,[21] S. Okuno,[14] S. L. Olsen,[7] Y. Onuki,[28] W. Ostrowicz,[26] H. Ozaki,[8] P. Pakhlov,[12] H. Palka,[26] C. W. Park,[37] N. Parslow,[38] R. Pestotnik,[13] L. E. Piilonen,[48] M. Rozanska,[26] H. Sagawa,[8] Y. Sakai,[8] N. Sato,[21] T. Schietinger,[17] O. Schneider,[17] J. Schümann,[25] C. Schwanda,[11] A. J. Schwartz,[4] S. Semenov,[12] K. Senyo,[21] M. E. Sevior,[20] T. Shibata,[28] H. Shibuya,[40] B. Shwartz,[1] V. Sidorov,[1] J. B. Singh,[31] A. Somov,[4] N. Soni,[31] R. Stamen,[8] S. Stanič,[47,*] M. Starič,[13] K. Sumisawa,[30] T. Sumiyoshi,[45] S. Suzuki,[34] S. Y. Suzuki,[8] O. Tajima,[8] F. Takasaki,[8] K. Tamai,[8] N. Tamura,[28] M. Tanaka,[8] Y. Teramoto,[29] X. C. Tian,[32] K. Trabelsi,[7] T. Tsuboyama,[8] T. Tsukamoto,[8] S. Uehara,[8] T. Uglov,[12] K. Ueno,[25] S. Uno,[8] Y. Ushiroda,[8] K. E. Varvell,[38] S. Villa,[17] C. C. Wang,[25] C. H. Wang,[24] M. Watanabe,[28] Y. Watanabe,[44] B. D. Yabsley,[48] A. Yamaguchi,[42] H. Yamamoto,[42] Y. Yamashita,[27] M. Yamauchi,[8] J. Ying,[32] Y. Yusa,[42] C. C. Zhang,[10] J. Zhang,[8] L. M. Zhang,[35] Z. P. Zhang,[35] V. Zhilich,[1] and D. Žontar[18,13]

(Belle Collaboration)

[1]*Budker Institute of Nuclear Physics, Novosibirsk*
[2]*Chiba University, Chiba*
[3]*Chonnam National University, Kwangju*
[4]*University of Cincinnati, Cincinnati, Ohio 45221, USA*
[5]*University of Frankfurt, Frankfurt*
[6]*Gyeongsang National University, Chinju*
[7]*University of Hawaii, Honolulu, Hawaii 96822, USA*
[8]*High Energy Accelerator Research Organization (KEK), Tsukuba*
[9]*Hiroshima Institute of Technology, Hiroshima*
[10]*Institute of High Energy Physics, Chinese Academy of Sciences, Beijing*
[11]*Institute of High Energy Physics, Vienna*
[12]*Institute for Theoretical and Experimental Physics, Moscow*
[13]*J. Stefan Institute, Ljubljana*
[14]*Kanagawa University, Yokohama*
[15]*Korea University, Seoul*
[16]*Kyungpook National University, Taegu*
[17]*Swiss Federal Institute of Technology of Lausanne, EPFL, Lausanne*
[18]*University of Ljubljana, Ljubljana*
[19]*University of Maribor, Maribor*
[20]*University of Melbourne, Victoria*
[21]*Nagoya University, Nagoya*
[22]*Nara Women's University, Nara*
[23]*National Central University, Chung-li*
[24]*National United University, Miao Li*
[25]*Department of Physics, National Taiwan University, Taipei*
[26]*H. Niewodniczanski Institute of Nuclear Physics, Krakow*
[27]*Nihon Dental College, Niigata*

[28]Niigata University, Niigata
[29]Osaka City University, Osaka
[30]Osaka University, Osaka
[31]Panjab University, Chandigarh
[32]Peking University, Beijing
[33]Princeton University, Princeton, New Jersey 08545, USA
[34]Saga University, Saga
[35]University of Science and Technology of China, Hefei
[36]Seoul National University, Seoul
[37]Sungkyunkwan University, Suwon
[38]University of Sydney, Sydney NSW
[39]Tata Institute of Fundamental Research, Bombay
[40]Toho University, Funabashi
[41]Tohoku Gakuin University, Tagajo
[42]Tohoku University, Sendai
[43]Department of Physics, University of Tokyo, Tokyo
[44]Tokyo Institute of Technology, Tokyo
[45]Tokyo Metropolitan University, Tokyo
[46]Tokyo University of Agriculture and Technology, Tokyo
[47]University of Tsukuba, Tsukuba
[48]Virginia Polytechnic Institute and State University, Blacksburg, Virginia 24061, USA
[49]Yonsei University, Seoul

(Received 10 November 2004; published 6 April 2005; corrected 19 April 2005)

We present a precise measurement of the standard model CP-violation parameter $\sin 2\phi_1$, the direct CP violation parameter $|\lambda|$, the lifetimes of charged and neutral B mesons and their ratio, and the B^0-$\overline{B}^0$ mixing parameter Δm_d based on a sample of 152×10^6 $B\overline{B}$ pairs collected at the $\Upsilon(4S)$ resonance with the Belle detector at the KEKB asymmetric-energy e^+e^- collider. One of two B mesons is fully reconstructed in a CP-eigenstate or a flavor-eigenstate decay channel. The flavor of the accompanying B meson is identified from its decay products. From the distributions of the time interval between the two B meson decay points, we obtain $\sin 2\phi_1 = 0.728 \pm 0.056(\text{stat}) \pm 0.023(\text{syst})$, $|\lambda| = 1.007 \pm 0.041(\text{stat}) \pm 0.033(\text{syst})$, $\tau_{B^0} = [1.534 \pm 0.008(\text{stat}) \pm 0.010(\text{syst})]$ ps, $\tau_{B^+} = [1.635 \pm 0.011(\text{stat}) \pm 0.011(\text{syst})]$ ps, $\tau_{B^+}/\tau_{B^0} = 1.066 \pm 0.008(\text{stat}) \pm 0.008(\text{syst})$ and $\Delta m_d = [0.511 \pm 0.005(\text{stat}) \pm 0.006(\text{syst})]$ ps^{-1}. The results for $\sin 2\phi_1$ and $|\lambda|$ are consistent with the standard model expectations. The significance of the observed deviation from unity in the lifetime ratio exceeds 5 standard deviations.

DOI: 10.1103/PhysRevD.71.072003 PACS numbers: 11.30.Er, 12.15.Hh, 13.25.Hw

I. INTRODUCTION

In the standard model (SM), CP violation arises from an irreducible phase in the weak interaction quark-mixing matrix (Cabibbo-Kobayashi-Maskawa (CKM) matrix) [1]. In particular, the SM predicts a CP-violating asymmetry in the time-dependent rates for B^0 and $\overline{B}^0$ decays to a common CP eigenstate f_{CP}, where the transition is dominated by the $b \to c\bar{c}s$ process, with negligible corrections from strong interactions [2]:

$$A(t) \equiv \frac{\Gamma[\overline{B}^0(t) \to f_{CP}] - \Gamma[B^0(t) \to f_{CP}]}{\Gamma[\overline{B}^0(t) \to f_{CP}] + \Gamma[B^0(t) \to f_{CP}]} = -\xi_f \sin 2\phi_1 \sin(\Delta m_d t), \quad (1)$$

where $\Gamma[B^0(t), \overline{B}^0(t) \to f_{CP}]$ is the rate for B^0 or $\overline{B}^0$ decay to f_{CP} at a proper-time t after production, ξ_f is the CP eigenvalue of f_{CP}, Δm_d is the mass difference between the two B^0 mass eigenstates, and ϕ_1 is one of the three interior angles of the CKM unitarity triangle, defined as $\phi_1 \equiv \pi - \arg(V_{tb}^* V_{td}/V_{cb}^* V_{cd})$. Nonzero values for $\sin 2\phi_1$ have been reported by the Belle and BaBar collaborations [3–5]. Belle's latest published measurement of $\sin 2\phi_1$ is based on a 78 fb^{-1} data sample (data set I) containing 85×10^6 $B\overline{B}$ pairs produced at the $\Upsilon(4S)$ resonance. In this paper, we report an improved measurement incorporating an additional 62 fb^{-1} (data set II) for a total of 140 fb^{-1} (152×10^6 $B\overline{B}$ pairs). A precise knowledge of $\sin 2\phi_1$ is essential for testing the Kobayashi-Maskawa model of CP violation.

The $\sin 2\phi_1$ measurement requires a determination of a proper-time resolution function and of the wrong-tag fractions using a large sample of exclusively reconstructed flavor-eigenstate decays. We perform a precise measurement of the mixing parameter Δm_d and of the neutral (charged) B meson lifetime τ_{B^0} (τ_{B^+}) as a by-product of this procedure. Our previous results are based on a 29.1 fb^{-1} data sample [6–8]; thus our new measurements with a 140fb^{-1} data sample provide significant improvements.

Changes exist in the analysis with respect to our earlier results. We apply a new proper-time resolution function

*On leave from Nova Gorica Polytechnic, Nova Gorica

that reduces systematic uncertainties. We introduce b-flavor-dependent wrong-tag fractions to accommodate possible differences between B^0 and $\overline{B}^0$ decays. We also adopt a multiparameter fit to the flavor-eigenstate samples to obtain Δm_d, τ_{B^0}, τ_{B^+}, the resolution parameters and wrong-tag fractions simultaneously. There are other improvements in the estimation of background components that are made possible by the increased statistics.

The data were collected with the Belle detector [9] at the KEKB asymmetric-energy e^+e^- collider [10], which collides 8.0 GeV e^- on 3.5 GeV e^+ at a small ($\pm$ 11 mrad) crossing angle. We use events where one of the B mesons decays to f_{CP} at time t_{CP}, and the other decays to a self-tagging state $f_{\rm tag}$, which distinguishes B^0 from $\overline{B}^0$, at time $t_{\rm tag}$. The CP violation manifests itself as an asymmetry $A(\Delta t)$, where Δt is the proper-time interval between the two decays: $\Delta t \equiv t_{CP} - t_{\rm tag}$. We also use events in which f_{CP} is replaced by a flavor eigenstate $f_{\rm flv}$; the decay chain in this case is $\Upsilon(4S) \to B^0\overline{B}^0 \to f_{\rm flv}f_{\rm tag}$. The time evolution is described as $e^{-|\Delta t|/\tau_{B^0}}/(4\tau_{B^0})\{1 \pm \cos(\Delta m_d \Delta t)\}$, where the plus (minus) sign is taken when the flavor of one B meson is opposite to (the same as) the other.

At KEKB, the $\Upsilon(4S)$ resonance is produced with a boost of $\beta\gamma = 0.425$ nearly along the z axis defined as antiparallel to the positron beam direction, and Δt can be determined as $\Delta t \simeq \Delta z/(\beta\gamma c)$, where Δz is the z distance between the f_{CP} and $f_{\rm tag}$ decay vertices, $\Delta z \equiv z_{CP} - z_{\rm tag}$. The average value of Δz is approximately 200 μm.

The Belle detector [9] is a large-solid-angle spectrometer that includes a silicon vertex detector (SVD), a central drift chamber (CDC), an array of aerogel threshold Čerenkov counters (ACC), time-of-flight (TOF) scintillation counters, and an electromagnetic calorimeter (ECL) comprised of CsI(Tl) crystals, all located inside a superconducting solenoid coil that provides a 1.5 T magnetic field. An iron flux-return located outside of the coil is instrumented to detect K_L^0 mesons and to identify muons (KLM).

II. EVENT SELECTION AND RECONSTRUCTION

A. Reconstruction of $B^0 \to$ charmonium $K^{(*)0}$ decays

We reconstruct B^0 decays to the following CP eigenstates [11]: $J/\psi K_S^0$, $\psi(2S)K_S^0$, $\chi_{c1}K_S^0$, $\eta_c K_S^0$ for $\xi_f = -1$ and $J/\psi K_L^0$ for $\xi_f = +1$. We also use $B^0 \to J/\psi K^{*0}$ decays with the subsequent decay $K^{*0} \to K_S^0\pi^0$. Here the final state is a mixture of even and odd CP, depending on the relative orbital angular momentum of the J/ψ and K^{*0}. We find that the final state is primarily $\xi_f = +1$; the $\xi_f = -1$ fraction is $0.19 \pm 0.02(\text{stat}) \pm 0.03(\text{syst})$ [12].

The reconstruction and selection criteria for all f_{CP} channels used in the measurement are described in detail elsewhere [3]. J/ψ and $\psi(2S)$ mesons are reconstructed via their decays to $\ell^+\ell^-$ ($\ell = \mu, e$). The $\psi(2S)$ is also reconstructed via $J/\psi\pi^+\pi^-$, and the χ_{c1} via $J/\psi\gamma$. The η_c is detected in the $K_S^0K^-\pi^+$, $K^+K^-\pi^0$, and $p\overline{p}$ modes. For the $J/\psi K_S^0$ mode, we use $K_S^0 \to \pi^+\pi^-$ and $\pi^0\pi^0$ decays; for other modes we only use $K_S^0 \to \pi^+\pi^-$. For reconstructed $B \to f_{CP}$ candidates other than $J/\psi K_L^0$, we identify B decays using the energy difference $\Delta E \equiv E_B^{\rm cms} - E_{\rm beam}^{\rm cms}$ and the beam-energy constrained mass $M_{\rm bc} \equiv \sqrt{(E_{\rm beam}^{\rm cms})^2 - (p_B^{\rm cms})^2}$, where $E_{\rm beam}^{\rm cms}$ is the beam energy in the center-of-mass system (cms) of the $\Upsilon(4S)$ resonance, and $E_B^{\rm cms}$ and $p_B^{\rm cms}$ are the cms energy and momentum of the reconstructed B candidate, respectively.

Candidate $B^0 \to J/\psi K_L^0$ decays are selected by requiring ECL and/or KLM hit patterns that are consistent with the presence of a shower induced by a K_L^0 meson. The centroid of the shower is required to be within a 45° cone centered on the K_L^0 direction inferred from two-body decay kinematics and the measured four-momentum of the J/ψ.

B. Reconstruction of flavor-eigenstate samples

1. $B^0 \to D^{*-}\ell^+\nu$

We use the decay chain $B^0 \to D^{*-}\ell^+\nu$, $D^{*-} \to \overline{D}^0\pi^-$, where $\overline{D}^0 \to K^+\pi^-$, $K^+\pi^-\pi^0$ or $K^+\pi^-\pi^+\pi^-$. We require associated SVD hits and radial impact parameters $dr < 0.2$ cm for all tracks. Track momenta in the laboratory frame for $\overline{D}^0 \to K^+\pi^-\pi^+\pi^-$ decays are required to be larger than 0.2 GeV/c, while no additional requirements are applied for the other modes. Charged kaons are identified by combining information from the TOF, ACC and dE/dx measurements in the CDC. Photon candidates are defined as isolated ECL clusters of more than 20 MeV that are not matched to any charged track. π^0 candidates are reconstructed from pairs of photon candidates with invariant masses between 124 and 146 MeV/c^2. A mass-constrained fit is performed to improve the π^0 momentum resolution. A minimum π^0 momentum of 0.2 GeV/c is required. For $\overline{D}^0 \to K^+\pi^-$ and $K^+\pi^-\pi^+\pi^-$ candidates, we use daughter combinations that have an invariant mass within 0.013 GeV/c^2 of m_{D^0}; for $\overline{D}^0 \to K^+\pi^-\pi^0$ we expand the mass window to -0.037 GeV/c^2 and $+0.023$ GeV/c^2. For $D^{*-} \to \overline{D}^0\pi^-$ decays, we combine $\overline{D}^0$ candidates with a low-momentum π^- (slow pion) that is reconstructed using a vertex constraint and require the mass difference between the D^{*-} and $\overline{D}^0$ candidates, $M_{\rm diff}$, to be within 1 MeV/c^2 of the nominal value. We reject D^{*-} candidates with cms momentum greater than 2.6 GeV/c, which is beyond the kinematic limit for B meson decays.

For the associated lepton, we use electrons or muons with a charge opposite to that of the D^{*-} candidate. Electron identification is based on a combination of CDC dE/dx information, the ACC response, and the energy deposition of the associated ECL shower. Muons are identified by comparing information from the KLM to extrapolated charged particle trajectories. We require $1.4 \text{ GeV}/c < p_\ell^{\rm cms} < 2.4 \text{ GeV}/c$, where $p_\ell^{\rm cms}$ is the cms momentum of the lepton. The cms angle of the lepton with

respect to the direction of the D^{*-} candidate is also required to be greater than 90°. For $B^0 \to D^{*-}\ell^+\nu$ decays, the energies and momenta of the B meson and the $D^*\ell$ system in the cms satisfy $M_\nu^2 = (E_B^{\rm cms} - E_{D^*\ell}^{\rm cms})^2 - |\vec{p}_B^{\rm cms}|^2 - |\vec{p}_{D^*\ell}^{\rm cms}|^2 + 2|\vec{p}_B^{\rm cms}||\vec{p}_{D^*\ell}^{\rm cms}|\cos\theta_{B,D^*\ell}$, where M_ν is the neutrino mass and $\theta_{B,D^*\ell}$ is the angle between $\vec{p}_B^{\rm cms}$ and $\vec{p}_{D^*\ell}^{\rm cms}$. We calculate $\cos\theta_{B,D^*\ell}$ setting $M_\nu = 0$. The signal region is defined as $|\cos\theta_{B,D^*\ell}| < 1.1$. We also require the candidate $D^{*-}\ell^+\nu$ decays to be outside the signal region when we artificially reverse the lepton momentum vector; this ensures that entries in the signal region after the reversal, which are used for the background estimation, do not contain $D^{*-}\ell^+\nu$ events.

2. Hadronic modes

B^0 and B^+ mesons are fully reconstructed in the following decay modes: $B^0 \to D^-\pi^+$, $D^{*-}\pi^+$, $D^{*-}\rho^+$, $J/\psi K^{*0}$, $B^+ \to \overline{D}^0\pi^+$, and $J/\psi K^+$. We also use $B^0 \to J/\psi K_S^0$ decays, which are described in the previous section, with no flavor assignment. D^{*-} and $\overline{D}^0$ candidates are reconstructed in the same decay modes that are used for the $D^{*-}\ell^+\nu$ mode. Charged D candidates are reconstructed in the $D^- \to K^+\pi^-\pi^-$ channel. For D and D^{*-} candidates, we apply mode-dependent requirements on the reconstructed D mass (ranging from ± 15 MeV/c^2 to ± 50 MeV/c^2) and the $M_{\rm diff}$ (ranging from ± 3 MeV/c^2 to ± 12 MeV/c^2), in a similar way as for the $D^{*-}\ell^+\nu$ mode. Candidate $K^{*0} \to K^+\pi^-$ decays are required to have an invariant mass within 75 MeV/c^2 of the nominal K^{*0} mass. ρ^+ candidates are selected as $\pi^+\pi^0$ pairs having invariant masses within 150 MeV/c^2 of the nominal ρ^+ mass.

To reduce background from $e^+e^- \to q\bar{q}$ ($q = u, d, s$ or c) continuum events, a selection based on the ratio of the second to zeroth Fox-Wolfram moments [13] and the angle between the thrust axes of the reconstructed and associated B mesons is applied mode by mode.

C. Flavor tagging

For neutral B to f_{CP} and $f_{\rm flv}$ decays, charged leptons, pions, kaons, and Λ baryons that are not associated with the reconstructed decay are used to identify the b-flavor of the accompanying B meson. The tagging algorithm is described in detail elsewhere [14]. We use two parameters, q and r, to represent the tagging information. The first, q, has the discrete value $+1$ (-1) when the tag-side B meson is likely to be a B^0 ($\overline{B}^0$). The parameter r corresponds to an event-by-event flavor-tagging dilution that ranges from $r = 0$ for no flavor discrimination to $r = 1$ for an unambiguous flavor assignment. It is determined from a large number of events generated by Monte Carlo (MC) simulation, and is used only to sort data into six intervals of r, according to estimated flavor purity. We determine directly from data the average wrong-tag probabilities, $w_l \equiv (w_l^+ + w_l^-)/2$ ($l = 1, 6$), and differences between B^0 and $\overline{B}^0$ decays, $\Delta w_l \equiv w_l^+ - w_l^-$, where $w_l^{+(-)}$ is the wrong-tag probability for the $B^0(\overline{B}^0)$ decay in each r interval.

D. Vertex reconstruction

The vertex position for the f_{CP} decay is reconstructed using leptons from J/ψ decays or charged hadrons from η_c decays. Each vertex position is required to be consistent with the interaction-region profile (IP), determined run-by-run, smeared in the r-ϕ plane to account for the B meson decay length. With the IP constraint, we are able to determine a vertex even with a single track; the fraction of single-track vertices is about 10% for z_{CP}.

The vertex position for the $f_{\rm flv}$ decay that includes a D meson in its decay products is reconstructed using the D meson trajectory, a track other than the slow π^- candidate from D^{*-} decay, and the IP constraint. For the $B^+ \to J/\psi K^+$ and $B^0 \to J/\psi K^{*0}(K^+\pi^-)$ decays, we use leptons from J/ψ decays and the IP constraint, in the same way as for the f_{CP} decay.

The vertex position for the $f_{\rm tag}$ is obtained with the IP constraint and with well reconstructed tracks that are not assigned to f_{CP} or $f_{\rm flv}$. The algorithm is described in detail elsewhere [15]. The fraction of single-track vertices is about 22% for $z_{\rm tag}$.

We only use events with vertices that satisfy $|\Delta t| < 70$ ps and $\xi < 100$, where ξ is the χ^2 of the vertex fit calculated only in the z direction [15]. The overall vertex reconstruction efficiency is $87.1 \pm 0.7\%$ for $B^0 \to J/\psi K_S^0$ candidates.

The proper-time interval resolution function $R_{\rm sig}(\Delta t)$ is formed by convolving four components: the detector resolutions for z_{CP} and $z_{\rm tag}$, the shift in the $z_{\rm tag}$ vertex position due to secondary tracks originating from charmed particle decays, and the kinematic approximation that the B mesons are at rest in the cms [15]. A small component of broad outliers in the Δz distribution, caused by misreconstruction, is represented by a Gaussian function.

E. Signal yields

After flavor tagging and vertexing, we find 5417 f_{CP} candidates in total in the signal region; these are used for the $\sin 2\phi_1$ determination. Table I lists the numbers of candidates, $N_{\rm ev}$, and the estimated signal purity for each f_{CP} mode. Figure 1 shows the $M_{\rm bc}$ distribution after applying mode-dependent requirements on ΔE for all B^0 candidates except for $B^0 \to J/\psi K_L^0$. There are 3085 total entries in the signal region defined as $5.27\ {\rm GeV}/c^2 < M_{\rm bc} < 5.29\ {\rm MeV}/c^2$. Figure 2 shows the $p_B^{\rm cms}$ distribution for $B^0 \to J/\psi K_L^0$ candidates. We find 2332 entries in the $0.20\ {\rm GeV}/c \le p_B^{\rm cms} \le 0.45\ {\rm GeV}/c$ signal region.

TABLE I. Numbers of reconstructed $B \to f_{CP}$ candidates after flavor tagging and vertex reconstruction, $N_{\rm ev}$, and the estimated signal purity, p.

Mode	ξ_f	$N_{\rm ev}$	p
$J/\psi K^0_S(\pi^+\pi^-)$	-1	1997	0.976 ± 0.001
$J/\psi K^0_S(\pi^0\pi^0)$	-1	288	0.82 ± 0.02
$\psi(2S)(\ell^+\ell^-)K^0_S$	-1	145	0.93 ± 0.01
$\psi(2S)(J/\psi\pi^+\pi^-)K^0_S$	-1	163	0.88 ± 0.01
$\chi_{c1}(J/\psi\gamma)K^0_S$	-1	101	0.92 ± 0.01
$\eta_c(K^0_S K^-\pi^+)K^0_S$	-1	123	0.72 ± 0.03
$\eta_c(K^+K^-\pi^0)K^0_S$	-1	74	0.70 ± 0.04
$\eta_c(p\overline{p})K^0_S$	-1	20	0.91 ± 0.02
All with $\xi_f = -1$	-1	2911	0.933 ± 0.002
$J/\psi K^{*0}(K^0_S\pi^0)$	$+1(81\%)$	174	0.93 ± 0.01
$J/\psi K^0_L$	$+1$	2332	0.63 ± 0.03

Table II lists $N_{\rm ev}$ and the purity for each $f_{\rm flv}$ mode after the vertexing. The total number of $f_{\rm flv}$ candidates is 177368 with a purity of 81%. Figure 3 shows the $\cos\theta_{B,D^*\ell}$ distribution for the $D^{*-}\ell^+\nu$ candidates. Figure 4 shows the $M_{\rm bc}$ distributions for B^0 and B^+ decays to $f_{\rm flv}$ states.

According to a MC simulation study, there is a small fraction of background (less than 1% for f_{CP} and 3% for $f_{\rm flv}$ candidates) from other B decays peaking in the $M_{\rm bc}$ signal region. The effect of the peaking background is treated as a systematic error.

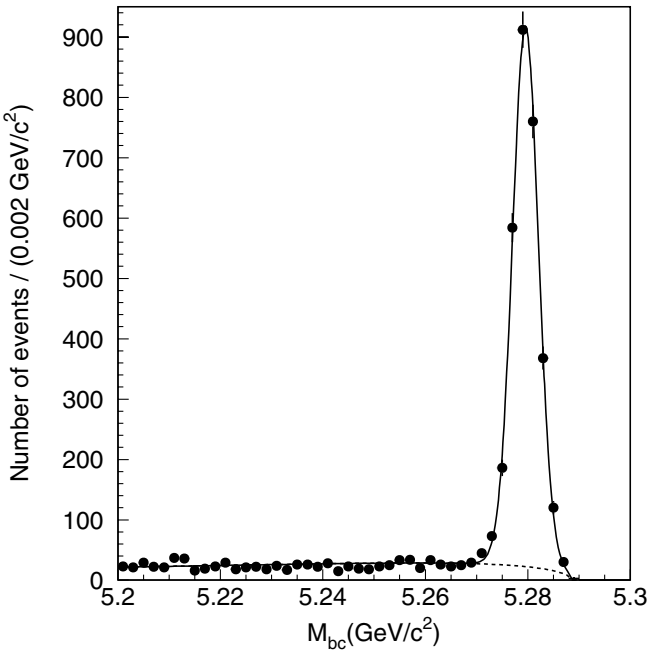

FIG. 1. Beam-energy constrained mass distribution within the ΔE signal region for all f_{CP} modes other than $J/\psi K^0_L$. The solid curve shows the fit to signal plus background distributions, and the dashed curve shows the background contribution.

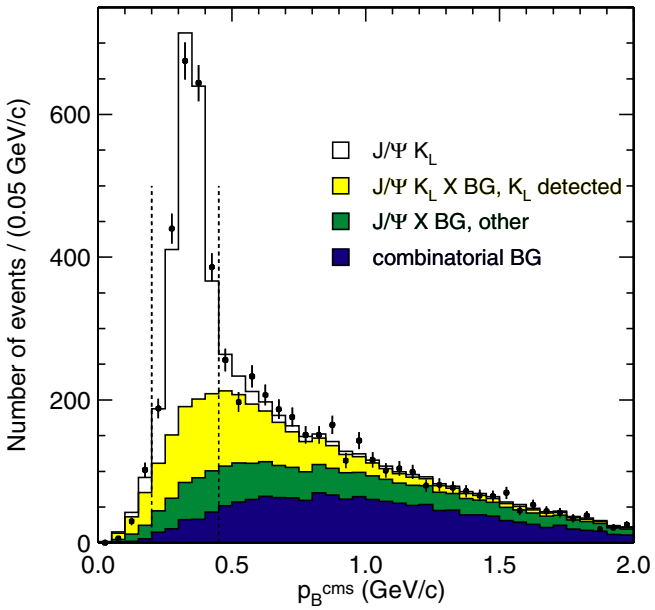

FIG. 2 (color online). $p_B^{\rm cms}$ distribution for $B^0 \to J/\psi K^0_L$ candidates with the results of the fit. The dashed lines indicate the signal region.

III. FIT RESULTS WITH FLAVOR-EIGENSTATE SAMPLES

We perform a multiparameter fit to flavor-eigenstate samples to obtain the B meson lifetimes, the B^0-$\overline{B}^0$ mixing parameter Δm_d, wrong-tag fractions, and parameters for the resolution function simultaneously. We use $B^0 \to D^{*-}\ell^+\nu$, $J/\psi K^{*0}(K^+\pi^-)$, $D^{*-}\pi^+$, $D^-\pi^+$, $D^{*-}\rho^+$, and $J/\psi K^0_S(\ell^+\ell^-)$ (for τ_{B^0} and resolution parameters only) for B^0 decays, and $B^+ \to \overline{D}^0\pi^+$ and $J/\psi K^+$ for B^+ decays. The fit uses 32 parameters; 12 for wrong-tag fractions, 14 for the resolution function, 3 for the B^+ background in B^0 decays, and 3 physics parameters Δm_d, τ_{B^0} and τ_{B^+}. We

TABLE II. Numbers of reconstructed $B \to f_{\rm flv}$ candidates after vertex reconstruction, $N_{\rm ev}$, and the estimated signal purity, p. $J/\psi K^0_S$ candidates are used with no flavor assignment.

Mode	$N_{\rm ev}$	p
$D^{*-}\ell^+\nu$	84823	0.781
$D^{*-}\pi^+$	11921	0.888
$D^-\pi^+$	11156	0.899
$D^{*-}\rho^+$	8767	0.763
$J/\psi K^{*0}(K^+\pi^-)$	3681	0.954
$J/\psi K^0_S(\pi^+\pi^-)$	2001	0.976
B^0 total	122349	0.809
$\overline{D}^0\pi^+$	46248	0.783
$J/\psi K^+$	8771	0.966
B^+ total	55019	0.812
$B^0 + B^+$ total	177368	0.810

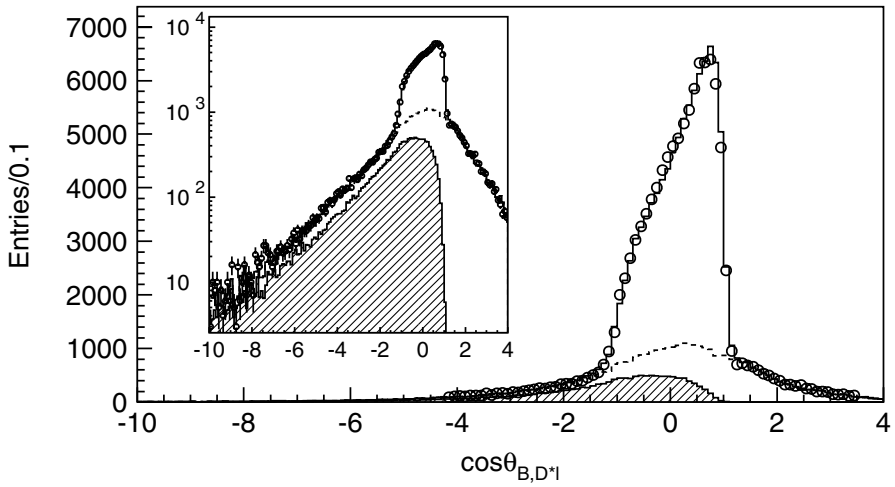

FIG. 3. $\cos\theta_{B,D^*\ell}$ distribution for the $D^{*-}\ell^+\nu$ candidates. The circles with errors show the data. The solid line is the fit result. The total background and the $D^{**}\ell\nu$ component are shown by the dashed line and the hatched area, respectively. The inset shows the same figure with a logarithmic vertical scale.

also obtain the lifetime ratio, $r_{\tau_B} \equiv \tau_{B^+}/\tau_{B^0}$, by repeating the fit in which τ_{B^+} is replaced with $r_{\tau_B}\tau_{B^0}$. Two of the 14 parameters for the resolution function are newly added to the resolution function described in [15] to improve the description of the effect of charmed particle decays on the $f_{\rm tag}$ vertex.

The probability density function (PDF) expected for the signal distribution for B^0 decays to $f_{\rm flv}$ is given by

$$\mathcal{P}_{\rm mix}^{\rm OF[SF]}(\Delta t, q, w_l, \Delta w_l) = \frac{e^{-|\Delta t|/\tau_{B^0}}}{8\tau_{B^0}}\{1 - q\Delta w_l + [-](1-2w_l)\cos(\Delta m_d \Delta t)\}, \quad (2)$$

where OF (SF) denotes $B^0\overline{B}^0$ (B^0B^0 or $\overline{B}^0\overline{B}^0$), i.e. a state with the opposite (same) flavor. The signal PDF for B^+ decays is given by

$$\mathcal{P}_{\rm sig}^{B^+}(\Delta t) = \frac{e^{-|\Delta t|/\tau_{B^+}}}{2\tau_{B^+}}. \quad (3)$$

The signal PDFs are convolved with the $R_{\rm sig}(\Delta t)$ to account for the detector resolution.

The background PDF for the hadronic modes is modeled as a sum of exponential and prompt components,

$$\mathcal{P}_{\rm bkg}(\Delta t) = (1 - f_\delta)\frac{e^{-|\Delta t|/\tau_{\rm bkg}}}{2\tau_{\rm bkg}} + f_\delta \delta(\Delta t), \quad (4)$$

$(1 - f_\delta)$ is the fraction of the exponential component with the effective lifetime $\tau_{\rm bkg}$, and $\delta(\Delta t)$ is the Dirac delta function. It is convolved with a sum of two Gaussians, which is used as the background resolution function. The parameters for the background PDF are determined using

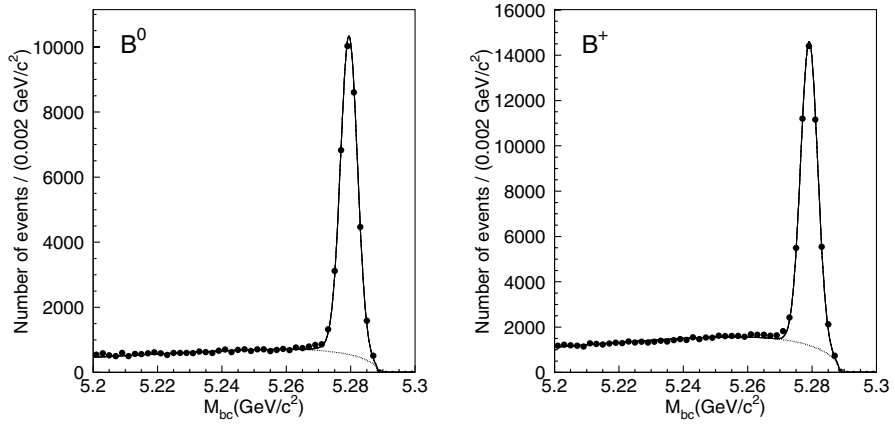

FIG. 4. Beam-energy constrained mass distributions in the ΔE signal region for flavor-eigenstate candidates in neutral B meson decays (left) and in charged B meson decays (right). The solid curves show the fits to signal plus background distributions and the dashed curves show the background contributions.

the ΔE-$M_{\rm bc}$ sideband region for each decay mode. For $B^+ \to \overline{D}^0\pi^+$ decays, using events outside the signal region, the value for f_δ is determined to be 0.49 ± 0.01 (0.45 ± 0.03) for events with multitrack (single-track) vertices and the effective lifetime $\tau_{\rm bkg}$ is found to be 0.93 ± 0.03 ps. The parameters for other $B \to f_{\rm flv}$ decays that include a D meson as a decay product are similar to those for the $B^+ \to \overline{D}^0\pi^+$ decay. A similar procedure for $B^+ \to J/\psi K^+$ decays yields $f_\delta = 0.86 \pm 0.05$ (0.75 ± 0.08) for events with multitrack (single-track) vertices and $\tau_{\rm bkg} = 1.55 \pm 0.22$ ps. The parameters for $B^0 \to J/\psi K^0_S$ are similar to those for $B^+ \to J/\psi K^+$. The value for f_δ in $B^0 \to J/\psi K^{*0}(K^+\pi^-)$ decays is found to be small; f_δ is 0.07 ± 0.05 for events with multitrack vertices and is fixed at zero for events with single-track vertices. The effective lifetime $\tau_{\rm bkg}$ is 1.50 ± 0.05 ps.

The background for the $D^{*-}\ell^+\nu$ decay is divided into four components: $B \to D^{**}\ell\nu$ events ($8.7 \pm 0.3\%$); fake D^* mesons ($8.0 \pm 0.1\%$); random combination of D^* mesons with leptons with no angular correlation called "uncorrelated background" ($2.5 \pm 0.1\%$); continuum events ($2.7 \pm 0.2\%$). Here D^{**} consists of charmed mesons heavier than the D^* meson and nonresonant $D^*\pi$ components. The PDF for the $B \to D^{**}\ell\nu$ background is given by a sum of B^0 and B^+ components,

$$\mathcal{P}^{OF[SF]}_{D^{**}\ell\nu}(\Delta t) = (1 - f_{B^+})\mathcal{P}^{OF[SF]}_{\rm mix} + f_{B^+}\mathcal{P}^{OF[SF]}_{B^+}, \quad (5)$$

where f_{B^+} is the B^+ fraction in the $B \to D^{**}\ell\nu$ background. The $\mathcal{P}^{\rm OF[SF]}_{B^+}$ is given by $\mathcal{P}^{\rm OF}_{B^+}(\Delta t) = (1 - w^l_{B^+})P^{B+}_{\rm bkg}(\Delta t)$ and $\mathcal{P}^{\rm SF}_{B^+}(\Delta t) = w^l_{B^+}P^{B+}_{\rm bkg}(\Delta t)$, where $w^l_{B^+}$ is the wrong-tag fraction determined from the $B^+ \to \overline{D}^0\pi^+$ sample and $\mathcal{P}^{B^+}_{\rm bkg}$ is given by

$$\mathcal{P}^{B^+}_{\rm bkg}(\Delta t) = (1 - f_{\tau'_{B^+}})\frac{e^{-|\Delta t|/\tau_{B^+}}}{4\tau_{B^+}} + f_{\tau'_{B^+}}\frac{e^{-|\Delta t|/\tau'_{B^+}}}{4\tau'_{B^+}}. \quad (6)$$

Here $f_{\tau'_{B^+}}$ and τ'_{B^+} are the fraction and the effective lifetime for events in which an additional π^+ from the D^{**} decays contaminates the $f_{\rm tag}$ vertex reconstruction. The parameters f_{B^+}, $f_{\tau'_{B^+}}$ and τ'_{B^+} are determined in the final fit. To determine these parameters precisely, events in $-10 < \cos\theta_{B,D^*\ell} < -1.1$, where the $D^{**}\ell\nu$ background events are dominant, are also included in the fit. The fit yields $f_{B^+} = 0.51 \pm 0.04$, $f_{\tau'_{B^+}} = 0.56 \pm 0.10$ and $\tau'_{B^+} = 0.74 \pm 0.14$ ps.

For continuum and uncorrelated backgrounds, the same functional form as that of the hadronic background PDF is used. The parameters for continuum are determined from off-resonance data to be $f_\delta = 0.55 \pm 0.09$ (0.58 ± 0.11) for events with multitrack (single-track) vertices and $\tau_{\rm bkg} = 0.80 \pm 0.08$ ps. For the uncorrelated background, a fit to the sample outside the signal region yields $f_\delta = 0.15 \pm 0.08$ and $\tau_{\rm bkg} = 1.23 \pm 0.06$ ps.

The PDF of the fake D^* background is given by Eq. (3) with a mixing component added to account for oscillation in the background. A fit to events in the $M_{\rm diff}$ sideband yields $f_\delta = 0.13 \pm 0.02$ (0.04 ± 0.03) for events with multitrack (single-track) vertices, $\tau_{\rm bkg} = 1.49 \pm 0.03$ ps and $\Delta m_{bkg} = 0.54 \pm 0.05$ ps^{-1}, where Δm_{bkg} is the effective mixing parameter. The fraction of the mixing component and wrong-tag fractions are determined for each of the six intervals of the flavor tag quality r. The wrong-tag fractions range from 0.50 ± 0.01 for the lowest r region to 0.20 ± 0.01 for the highest r region. The fraction of the mixing component for the lowest r region is fixed at 0. Values for the other r intervals range from 0.39 ± 0.12 to 0.84 ± 0.09.

We test the fit method and parameterization with a large number of MC events, and obtain results consistent with the input values. The wrong-tag fractions obtained with the MC events are also found to be correct.

The unbinned maximum-likelihood fit to data yields

$$\tau_{B^0} = [1.534 \pm 0.008(\text{stat}) \pm 0.010(\text{syst})]\ \text{ps}, \quad (7)$$

$$\tau_{B^+} = [1.635 \pm 0.011(\text{stat}) \pm 0.011(\text{syst})]\ \text{ps}, \quad (8)$$

$$\tau_{B^+}/\tau_{B^0} = 1.066 \pm 0.008(\text{stat}) \pm 0.008(\text{syst}), \quad (9)$$

$$\Delta m_d = [0.511 \pm 0.005(\text{stat}) \pm 0.006(\text{syst})]\ \text{ps}^{-1}. \quad (10)$$

The results are consistent with our previous measurements [6–8] and supersede them. Figure 5 shows the flavor asymmetry, $\mathcal{A}(\Delta t) = [\mathrm{N_{OF}}(\Delta t) - \mathrm{N_{SF}}(\Delta t)]/[\mathrm{N_{OF}}(\Delta t) +$

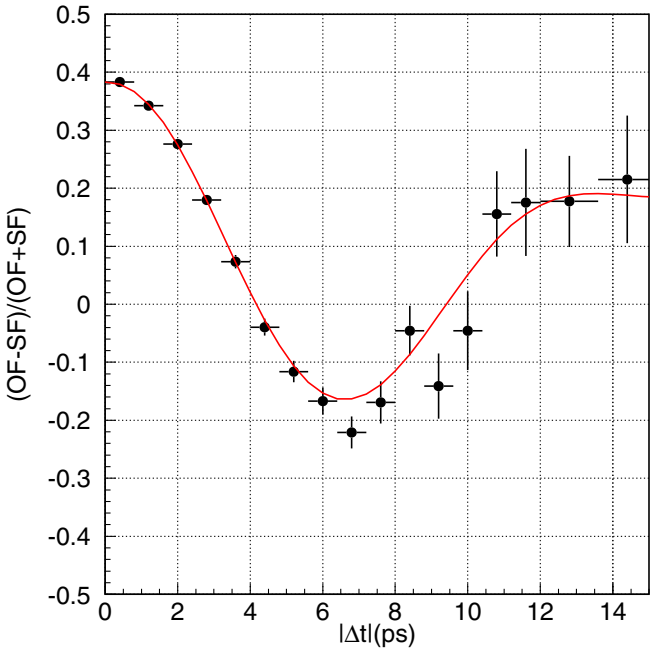

FIG. 5 (color online). Time-dependent flavor asymmetry for flavor-eigenstate decays. The curve is the result of the unbinned maximum-likelihood fit.

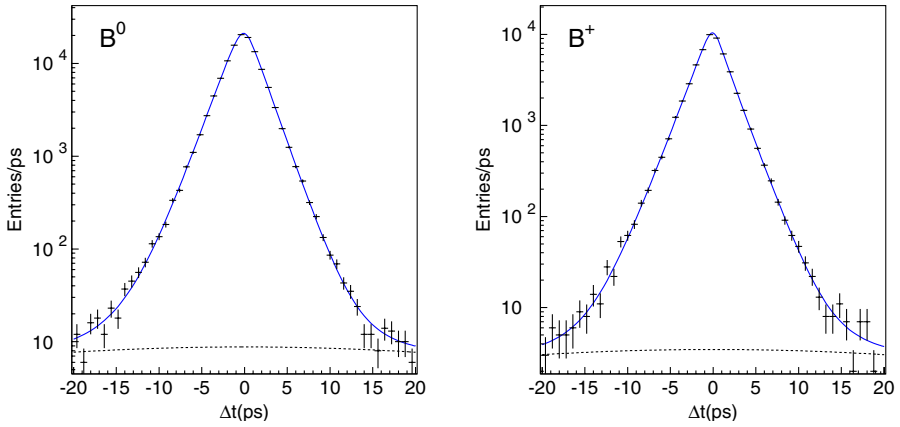

FIG. 6 (color online). Δt distributions of neutral B meson pairs (left) and charged B meson pairs (right). The solid lines represent the results of the unbinned maximum-likelihood fit. The dashed lines correspond to the outlier components.

TABLE III. Summary of the systematic errors on the measurement of τ_{B^0}, τ_{B^+}, τ_{B^+}/τ_{B^0} and Δm_d.

Source	τ_{B^0}	τ_{B^+}	τ_{B^+}/τ_{B^0}	Δm_d
Vertex reconstruction	0.005	0.007	0.003	0.003
Resolution function	0.004	0.005	0.004	0.001
Possible fit bias	0.003	0.004	0.003	0.002
$D^{**}\ell\nu$ background	0.004	0.003	0.002	0.004
Other background fraction	0.001	0.006	0.003	0.001
Background Δt shape	0.006	0.003	0.005	0.002
Total	0.010 (ps)	0.011 (ps)	0.008	0.006 (ps^{-1})

$N_{SF}(\Delta t)$], where $N_{OF(SF)}$ denotes the number of OF (SF) events. The results of the lifetime measurements for neutral and charged B meson decays are shown in Fig. 6.

Systematic uncertainties are listed in Table III. The method to determine the systematic errors due to the vertex reconstruction follows the same procedure as for the $\sin 2\phi_1$ measurement, which will be explained later. We estimate the contribution due to uncertainties in the resolution function by comparison of different parametrizations, as well as by changing parameters that are derived from MC to model the effect of nonprimary tracks [15]. A possible bias in the event reconstruction and fitting procedure is checked with a large number of MC events. We find no bias and take the statistical error in MC as a systematic error. Several D^{**} components are used in this analysis to model the $\cos\theta_{B,D^*\ell}$ shape for the $D^{**}\ell\nu$ background. To estimate the systematic errors due to uncertainties of the fractions of the D^{**} components, we set the fraction of each component to unity (with all other components set to zero) and repeat the analysis; for each measurement, we take the largest variation on the result as the systematic error. Systematic errors that arise from uncertainties in other background fractions and from the background Δt shape are obtained by varying each parameter individually, repeating the fit procedure, and adding each contribution in quadrature. In the nominal fit, we do not include a mixing component in the background PDF for the hadronic decays. We repeat the fit with a background PDF including a mixing term. Uncertainties in the overall z scale of the detector arising from the measurement error and thermal expansion during the operation are found to be negligible.

The same fit also yields wrong-tag fractions that are summarized in Table IV. The total effective tagging efficiency is determined to be $\epsilon_{\text{eff}} \equiv \sum_{l=1}^{6} \epsilon_l (1-2w_l)^2 = 0.287 \pm 0.005$, where ϵ_l is the event fraction for each r

TABLE IV. Event fractions ϵ_l, wrong-tag fractions w_l, wrong-tag fraction differences Δw_l, and average effective tagging efficiencies $\epsilon^l_{\text{eff}} = \epsilon_l(1-2w_l)^2$ for each r interval. The errors include both statistical and systematic uncertainties.

l	r interval	ϵ_l	w_l	Δw_l	ϵ^l_{eff}
1	0.000 – 0.250	0.398	0.464 ± 0.006	-0.011 ± 0.006	0.002 ± 0.001
2	0.250 – 0.500	0.146	0.331 ± 0.008	$+0.004 \pm 0.010$	0.017 ± 0.002
3	0.500 – 0.625	0.104	0.231 ± 0.009	-0.011 ± 0.010	0.030 ± 0.002
4	0.625 – 0.750	0.122	0.163 ± 0.008	-0.007 ± 0.009	0.055 ± 0.003
5	0.750 – 0.875	0.094	0.109 ± 0.007	$+0.016 \pm 0.009$	0.057 ± 0.002
6	0.875 – 1.000	0.136	0.020 ± 0.005	$+0.003 \pm 0.006$	0.126 ± 0.003

interval determined from the $J/\psi K^0_S$ simulation and is listed in Table IV. The error includes both statistical and systematic uncertainties.

We find that the average Δt resolution is $\sim$1.43 ps (rms). The width of the outlier component is determined to be (39 ± 2) ps; the fractions of the outlier components are $(2.1 \pm 0.6) \times 10^{-4}$ for events with both vertices reconstructed with more than one track, and $(3.1 \pm 0.1) \times 10^{-2}$ for events with at least one single-track vertex.

IV. RESULTS OF *CP* ASYMMETRY MEASUREMENTS

Figure 7 shows the observed Δt distributions for the $q\xi_f = +1$ and $q\xi_f = -1$ event samples (top), the asymmetry between two samples with $0 < r \leq 0.5$ (middle) and with $0.5 < r \leq 1.0$ (bottom). The asymmetry in the region $0.5 < r \leq 1.0$, where wrong-tag fractions are small as shown in Table IV, clearly demonstrates large *CP* violation.

We determine $\sin 2\phi_1$ from an unbinned maximum-likelihood fit to the observed Δt distributions. The PDF for the signal distribution is given by

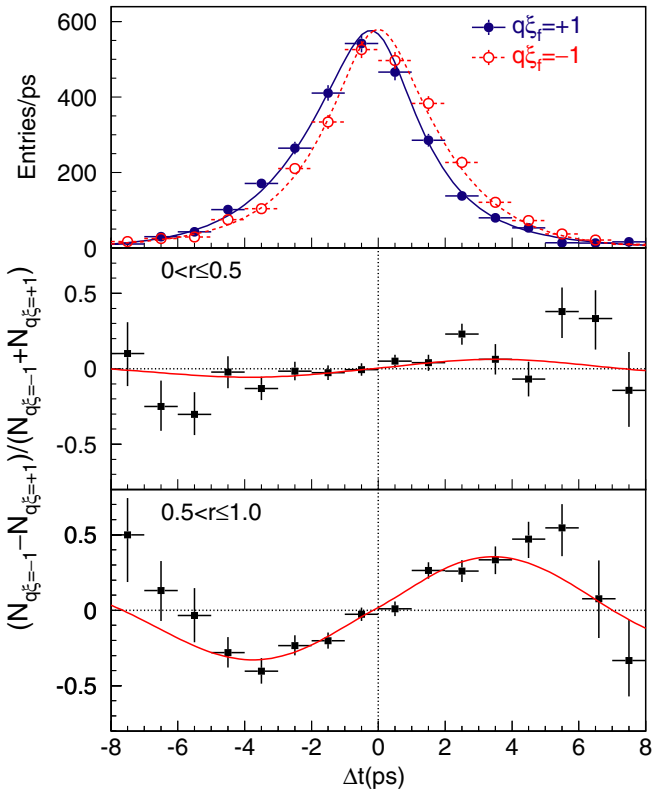

FIG. 7 (color online). Δt distributions for the events with $q\xi_f = -1$ (open points) and $q\xi_f = +1$ (solid points) with all modes combined (top), asymmetry between $q\xi_f = -1$ and $q\xi_f = +1$ samples with $0 < r \leq 0.5$ (middle), and with $0.5 < r \leq 1$ (bottom). The results of the global unbinned maximum-likelihood fit ($\sin 2\phi_1 = 0.728$) are also shown.

$$\mathcal{P}_{\rm sig}(\Delta t, q, w_l, \Delta w_l, \xi_f) = \frac{e^{-|\Delta t|/\tau_{B^0}}}{4\tau_{B^0}}[1 - q\Delta w_l - q\xi_f(1 - 2w_l)\sin 2\phi_1 \sin(\Delta m_d \Delta t)], \quad (11)$$

where we fix the B^0 lifetime τ_{B^0} and mass difference Δm_d at their world average values [16]. Each PDF is convolved with the appropriate $R_{\rm sig}(\Delta t)$ to determine the likelihood value for each event as a function of $\sin 2\phi_1$:

$$P_i = (1 - f_{\rm ol}) \int_{-\infty}^{+\infty} [f_{\rm sig}\mathcal{P}_{\rm sig}(\Delta t')R_{\rm sig}(\Delta t - \Delta t') + (1 - f_{\rm sig})\mathcal{P}_{\rm bkg}(\Delta t')R_{\rm bkg}(\Delta t - \Delta t')]d\Delta t' + f_{\rm ol}P_{\rm ol}(\Delta t), \quad (12)$$

where $f_{\rm sig}$ is the signal fraction calculated as a function of $p_B^{\rm cms}$ for $J/\psi K^0_L$ and of ΔE and $M_{\rm bc}$ for other modes. $\mathcal{P}_{\rm bkg}(\Delta t)$ is the PDF for combinatorial background events, which is modeled as a sum of exponential and prompt components. It is convolved with a sum of two Gaussians, $R_{\rm bkg}$, which is used as the background resolution function. We assume no asymmetry in the background Δt distribution.

For $B^0 \to J/\psi K^0_L$ and $J/\psi K^{*0}$ decays, in addition to the combinatorial background, background events from other B decays and their *CP* asymmetries are considered. The background in the $J/\psi K^0_L$ mode is dominated by the following $B \to J/\psi X$ decays: $J/\psi K^0_S$ having $\xi_f = -1$ $(10 \pm 2\%)$; $\psi(2S)K^0_L$, $\chi_{c1}K^0_L$ and $J/\psi\pi^0$ having $\xi_f = +1$ $(4 \pm 1\%)$; $J/\psi K^{*0}(K^{*0} \to K^0_L\pi^0)$ $(20 \pm 2\%)$, which is a mixture of $\xi_f = -1$ (81%) and $\xi_f = +1$ (19%); other non-*CP* modes $(66 \pm 1\%)$. The fraction of each component is obtained from a MC simulation study. For $J/\psi K^{*0}(K^0_S\pi^0)$ decays, we include in our PDF contaminations from other $B \to J/\psi K^*$ decays $(7.1 \pm 0.3\%)$ and nonresonant $B^0 \to J/\psi K^0_S\pi^0$ decays $(6.3 \pm 0.5\%)$ in the $M_{\rm bc}$ peak. The background fractions are obtained from MC and the K^* mass sideband [12]. We use the signal PDF with no *CP* asymmetry for these components.

To account for a small number of events that give large Δt in both the signal and background, we introduce the PDF of the outlier component, $P_{\rm ol}$, and its fraction $f_{\rm ol}$. The only free parameter in the final fit is $\sin 2\phi_1$, which is determined by maximizing the likelihood function $L = \prod_i P_i$, where the product is over all events. We obtain

$$\sin 2\phi_1 = 0.728 \pm 0.056(\text{stat}) \pm 0.023(\text{syst}). \quad (13)$$

The result is consistent with the value in our previous publication [4] and supersedes it with a reduced error.

The signal PDF for a neutral B meson decaying into a *CP* eigenstate [Eq. (11)] can be expressed in a more general form as

$$\mathcal{P}_{\rm sig}(\Delta t, q, w_l, \Delta w_l) = \frac{e^{-|\Delta t|/\tau_{B^0}}}{4\tau_{B^0}}\Big\{1 - q\Delta w_l + q(1 - 2w_l)[S\sin(\Delta m_d \Delta t) + \mathcal{A}\cos(\Delta m_d \Delta t)]\Big\}, \quad (14)$$

where $S \equiv 2\mathrm{Im}(\lambda)/(|\lambda|^2+1)$, $\mathcal{A} \equiv (|\lambda|^2-1)/(|\lambda|^2+1)$, and λ is a complex parameter that depends on both B^0-$\overline{B}^0$ mixing and on the amplitudes for B^0 and $\overline{B}^0$ decay to a CP eigenstate. The presence of the cosine term ($|\lambda| \neq 1$) would indicate direct CP violation; the value for $\sin 2\phi_1$ reported above is determined with the assumption $|\lambda| = 1$, as $|\lambda|$ is expected to be very close to 1 in the SM. In order to test this assumption, we also performed a fit using the expression above with $a_{CP} \equiv -\xi_f \mathrm{Im}(\lambda)/|\lambda|$ and $|\lambda|$ as free parameters, keeping everything else the same. We obtain

$$|\lambda| = 1.007 \pm 0.041(\mathrm{stat}) \pm 0.033(\mathrm{syst}), \quad (15)$$

and $a_{CP} = 0.728 \pm 0.056(\mathrm{stat})$. This result is consistent with the assumption of no direct CP violation used in our analysis and the a_{CP} term is in good agreement with the $\sin 2\phi_1$ value obtained with the one-parameter fit.

Table V lists the systematic errors on $\sin 2\phi_1$ and $|\lambda|$. The total systematic error is obtained by adding each of them in quadrature. The largest contribution for $\sin 2\phi_1$ comes from vertex reconstruction. The systematic error due to the IP constraint in the vertex reconstruction is estimated by varying ($\pm 10\mu$ m) the smearing used to account for the B flight length. The track selection criteria are also varied to search for possible systematic biases. The effect of the vertex quality cut is estimated by varying the cut to $\xi < 50$ and $\xi < 200$. We vary the $|\Delta t|$ range by ± 30 ps to estimate the systematic uncertainty due to the $|\Delta t|$ fit range. Small biases in the Δz measurement are observed in $e^+e^- \to \mu^+\mu^-$ and other control samples. Systematic errors are estimated by applying special correction functions to account for the observed biases, repeating the fit, and comparing the obtained values with the nominal results. Systematic errors due to imperfect SVD alignment are determined from MC samples that have artificial misalignment effects to reproduce impact-parameter resolutions observed in data. In these studies, whenever required, we repeat the fit to the $f_{\rm flv}$ samples, update resolution function parameters and wrong-tag fractions, and perform the fit to CP-eigenstate event samples using the updated parameters so that the uncertainties in question are treated in a consistent way.

TABLE V. Summary of the systematic errors on $\sin 2\phi_1$ and $|\lambda|$.

Source	$\sin 2\phi_1$	$\lvert\lambda\rvert$
Vertex reconstruction	0.013	0.012
Flavor tagging	0.007	0.008
Resolution function	0.008	0.004
Possible fit bias	0.008	0.006
Background fraction ($J/\psi K^0_L$)	0.011	0.003
Background fraction (except for $J/\psi K^0_L$)	0.007	0.007
Physics (τ_{B^0}, Δm_d, $J/\psi K^{*0}$)	0.003	0.001
Background Δt shape	0.002	0.001
Tag-side interference	0.002	0.028
Total	0.023	0.033

Systematic errors due to uncertainties in the wrong-tag fractions given in Table IV are studied by varying the wrong-tag fraction individually for each r region. Possible differences of the tagging performance between f_{CP} and $f_{\rm flv}$ events are estimated using MC events.

Systematic errors due to uncertainties in the resolution function are estimated by varying each resolution parameter obtained from data (MC) by $\pm 1\sigma$ ($\pm 2\sigma$), repeating the fit and adding each variation in quadrature. We also divide the entire data set into two and prepare two sets of resolution parameters to consider a possible difference in the detector performance. We repeat the fit with these resolution parameters and assign the difference from the nominal result as a systematic error. We also include other sources examined for the fit to the flavor-eigenstate samples, which are explained in the previous section.

A possible fit bias is examined by a fit to a large number of MC events. We find no bias and take the statistical error from the MC as a systematic error.

Systematic errors from uncertainties in the background fractions and in the background Δt shape are estimated by varying each background parameter obtained from data (MC) by $\pm 1\sigma$ ($\pm 2\sigma$). The systematic error due to CP content in the $J/\psi K^0_L$ backgrounds is checked by varying the parameters obtained from the MC by $\pm 2\sigma$.

The small peaking background in the $M_{\rm bc}$ signal region of f_{CP} modes other than $J/\psi K^{*0}$ is neglected in the nominal analysis. The effect of the fractions and their CP asymmetries is studied with MC simulation and is included in systematic errors.

Each physics parameter (τ_{B^0}, Δm_d, $J/\psi K^{*0}$ polarization) is also varied by its error; for Δm_d, we also use our result ($\Delta m_d = 0.511\ \mathrm{ps}^{-1}$), repeat the fit and take the larger change as the systematic error.

Finally, we investigate the effects of interference between CKM-favored and CKM-suppressed $B \to D$ transitions in the $f_{\rm tag}$ final state [17]. A small correction to the PDF for the signal distribution arises from the interference. We estimate the amount of correction using the $B^0 \to D^{*-}\ell^+\nu$ sample. We then generate MC pseudoexperiments and make an ensemble test to obtain systematic biases in $\sin 2\phi_1$ and $|\lambda|$. We find that the effect on $\sin 2\phi_1$ is negligibly small, while a possible shift

TABLE VI. Numbers of candidate events, N_{ev}, and values of $\sin 2\phi_1$, $|\lambda|$ for various subsamples (statistical errors only).

Sample	N_{ev}	$\sin 2\phi_1$	$\lvert\lambda\rvert$
$J/\psi K_S^0(\pi^+\pi^-)$	1997	0.67 ± 0.08	0.98 ± 0.06
$J/\psi K_S^0(\pi^0\pi^0)$	288	0.72 ± 0.20	1.18 ± 0.27
$\psi(2S)K_S^0$	308	0.89 ± 0.20	0.94 ± 0.14
$\chi_{c1}K_S^0$	101	1.54 ± 0.49	0.76 ± 0.22
$\eta_c K_S^0$	217	1.32 ± 0.28	1.10 ± 0.30
All with $\xi_f = -1$	2911	0.73 ± 0.06	0.99 ± 0.05
$J/\psi K_L^0$	2332	0.77 ± 0.13	1.04 ± 0.08
$J/\psi K^{*0}(K_S^0\pi^0)$	174	0.10 ± 0.45	1.11 ± 0.33
$f_{tag} = B^0$ $(q = +1)$	2717	0.72 ± 0.09	0.89 ± 0.09
$f_{tag} = \overline{B}^0$ $(q = -1)$	2700	0.74 ± 0.08	1.17 ± 0.11
$0 < r \leq 0.5$	2985	0.95 ± 0.26	1.18 ± 0.22
$0.5 < r \leq 0.75$	1224	0.68 ± 0.11	1.11 ± 0.09
$0.75 < r \leq 1$	1208	0.73 ± 0.07	0.95 ± 0.05
Data set I (78 fb $-$ 1)	3013	0.72 ± 0.07	0.95 ± 0.05
Data set II (62 fb $-$ 1)	2404	0.74 ± 0.09	1.09 ± 0.07
All	5417	0.728 ± 0.056	1.007 ± 0.041

in $|\lambda|$ becomes the largest contribution to the systematic error.

Several checks on the measurement are performed. Table VI lists the results obtained by applying the same analysis to various subsamples. All values are statistically consistent with each other. Figure 8 shows the raw asymmetries and the fit results for $(c\bar{c})K_S^0$ (top) and $J/\psi K_L^0$ (bottom). A fit to the non-*CP* eigenstate modes $B^0 \to D^{*-}\ell^+\nu$ and $J/\psi K^{*0}(K^+\pi^-)$, where no asymmetry is expected, yields "$\sin 2\phi_1$" $= 0.012 \pm 0.013$(stat).

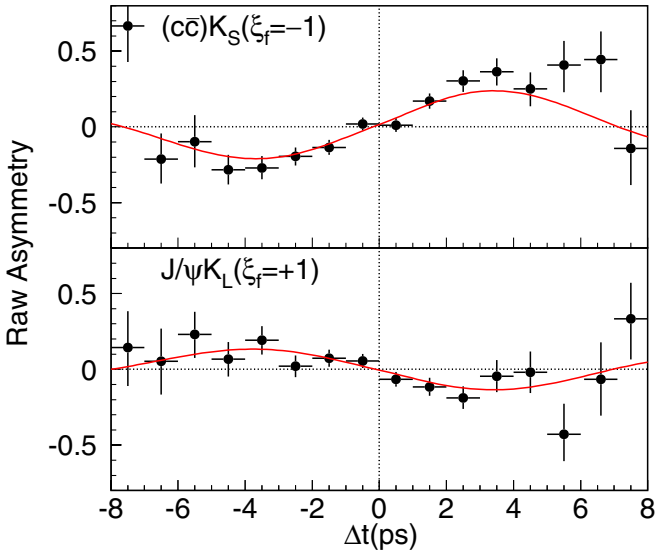

FIG. 8 (color online). Raw asymmetries for $(c\bar{c})K_S^0$ $(\xi_f = -1)$ (top) and $J/\psi K_L^0$ $(\xi_f = +1)$ (bottom). The curves are the results of the global unbinned maximum-likelihood fit.

V. SUMMARY

Using 152×10^6 $B\overline{B}$ pairs collected at the $\Upsilon(4S)$ resonance with the Belle detector at the KEKB asymmetric-energy e^+e^- collider, we have measured the *CP*-violation parameters $\sin 2\phi_1$ and $|\lambda|$, B meson lifetimes and their ratio, and the mixing parameter Δm_d. These are basic parameters of the standard model. The results are summarized as follows:

$$\begin{aligned}
\sin 2\phi_1 &= 0.728 \pm 0.056(\text{stat}) \pm 0.023(\text{syst}),\\
|\lambda| &= 1.007 \pm 0.041(\text{stat}) \pm 0.033(\text{syst}),\\
\tau_{B^0} &= [1.534 \pm 0.008(\text{stat}) \pm 0.010(\text{syst})]\ \text{ps},\\
\tau_{B^+} &= [1.635 \pm 0.011(\text{stat}) \pm 0.011(\text{syst})]\ \text{ps},\\
\tau_{B^+}/\tau_{B^0} &= 1.066 \pm 0.008(\text{stat}) \pm 0.008(\text{syst}),\\
\Delta m_d &= [0.511 \pm 0.005(\text{stat}) \pm 0.006(\text{syst})]\ \text{ps}^{-1}.
\end{aligned}$$

All results are significant improvements in precision from the previous measurements, and are in agreement with the standard model expectations. The significance of the observed deviation from unity in the lifetime ratio exceeds 5 standard deviations for the first time by a single measurement.

ACKNOWLEDGMENTS

We thank the KEKB group for the excellent operation of the accelerator, the KEK Cryogenics group for the efficient operation of the solenoid, and the KEK computer group and the National Institute of Informatics for valuable computing and Super-SINET network support. We acknowledge support from the Ministry of Education, Culture, Sports, Science, and Technology of Japan and the Japan Society for the Promotion of Science; the Australian Research Council and the Australian Department of Education, Science and Training; the National Science Foundation of China under contract No. 10175071; the Department of Science and Technology of India; the BK21 program of the Ministry of Education of Korea and the CHEP SRC program of the Korea Science and Engineering Foundation; the Polish State Committee for Scientific Research under contract No. 2P03B 01324; the Ministry of Science and Technology of the Russian Federation; the Ministry of Education, Science and Sport of the Republic of Slovenia; the Swiss National Science Foundation; the National Science Council and the Ministry of Education of Taiwan; and the U.S. Department of Energy.

[1] M. Kobayashi and T. Maskawa, Prog. Theor. Phys. **49**, 652 (1973).
[2] A. B. Carter and A. I. Sanda, Phys. Rev. D **23**, 1567 (1981); I. I. Bigi and A. I. Sanda, Nucl. Phys. **B193**, 85 (1981).
[3] Belle Collaboration, K. Abe *et al.*, Phys. Rev. Lett. **87**, 091802 (2001); Phys. Rev. D **66**, 032007 (2002).
[4] Belle Collaboration, K. Abe *et al.*, Phys. Rev. D **66**, 071102 (2002).
[5] BaBar Collaboration, B. Aubert *et al.*, Phys. Rev. Lett. **87**, 091801 (2001); Phys. Rev. D **66**, 032003 (2002); Phys. Rev. Lett. **89**, 201802 (2002); Phys. Rev. Lett. (to be published).
[6] Belle Collaboration, K. Abe *et al.*, Phys. Rev. Lett. **88**, 171801 (2002).
[7] Belle Collaboration, T. Tomura *et al.*, Phys. Lett. B **542**, 207 (2002).
[8] Belle Collaboration, K. Hara *et al.* Phys. Rev. Lett. **89**, 251803 (2002).
[9] Belle Collaboration, A. Abashian *et al.*, Nucl. Instrum. Methods Phys. Res., Sect. A **479**, 117 (2002).
[10] S. Kurokawa and E. Kikutani, Nucl. Instrum. Methods Phys. Res., Sect. A **499**, 1 (2003), and other papers included in this volume.
[11] In this paper the inclusion of charge conjugate state is implied.
[12] Belle Collaboration, K. Abe *et al.*, Phys. Lett. B **538**, 11 (2002).
[13] G. C. Fox and S. Wolfram, Phys. Rev. Lett. **41**, 1581 (1978).
[14] H. Kakuno *et al.*, Nucl. Instrum. Methods Phys. Res., Sect. A **533**, 516 (2004).
[15] H. Tajima *et al.*, Nucl. Instrum. Methods Phys. Res., Sect. A **533**, 370 (2004).
[16] Particle Data Group, S. Eidelman *et al.*, Phys. Lett. B **592**, 1 (2004).
[17] O. Long, M. Baak, R. N. Cahn, and D. Kirkby, Phys. Rev. D **68**, 034010 (2003).